Supplementary Information

DNA introduces an independent temperature responsiveness to thermosensitive microgels and enables switchable plasmon coupling as well as controlled uptake and release

Sabine Eisold,[a] Laura Hoppe Alvarez,[b] Ke Ran,[c] Rebecca Hengsbach,[a] Gerhard Fink,[a] Silvia Centeno Benigno,[b] Joachim Mayer,[c] Dominik Wöll and [b] Ulrich Simon[a]

[a] Institute of Inorganic Chemistry, RWTH Aachen University, 52074 Aachen, Germany

[b]Institute of Physical Chemistry, RWTH Aachen University, 52074 Aachen, Germany

[c] Central Facility for Electron Microscopy, RWTH Aachen University, 52074 Aachen, Germany

1. Synthesis of µGs

Syntheses were carried out in ultrapure water (ELGA Purelab Plus system from ELGA LabWater). The chemicals were purchased from commercial sources without further purification.

The pNIPMAM µGs were synthesized according to our previous published procedure[1] via precipitation polymerization with N,N'-bis(acryloyl)cystamine (BAC) as co-monomer[2] and N,N'-methylenebis(acrylamide) (BIS) as the cross-linker. They undergo a VPT at 42 °C in water (Figure S1, black).

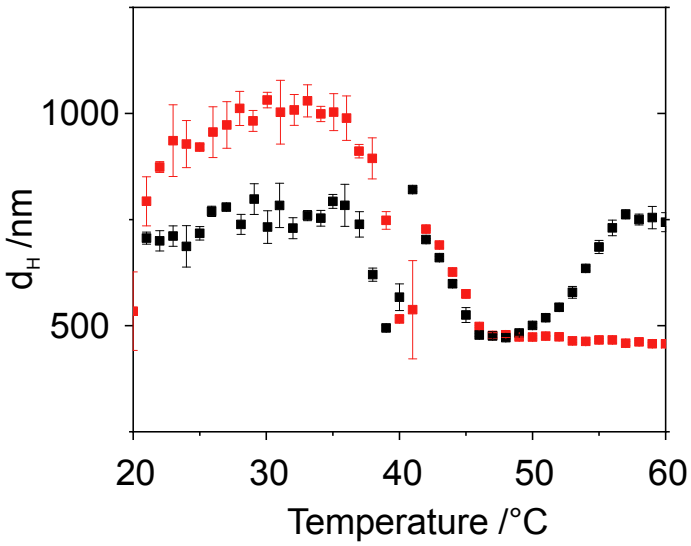

Figure S1: Temperature-dependent hydrodynamic diameter from DLS measurements of the non-functionalized µGs (black) and the DNA-functionalized µGs (red). Note that is some cases we observe an increase in diameter above the VPTT for the non-functionalized µGs, which we attribute to aggregation. This effect was not observed for the DNA-functionalized one, which we tentatively attribute to a better electrostatic stabilization.

^{1}H-NMR measurements on the µGs were performed on a Bruker Avance-II-400 MHz spectrometer equipped with a broadband observe probe. The temperature was controlled by a Bruker BVT-3200 unit. Samples were prepared as dispersions in deuterated water (D_2O) in 5 mm tubes. In order to follow the volume phase transition of the µG, from the swollen to the collapsed state, temperature dependent measurements in a range between 25 °C and 50 °C in 1 °C steps were performed on three samples with different sodium chloride concentrations (c(NaCl)=[0 M, 0.1 M, 1 M]). Each sample was measured twice crossing the temperature range from low-to-high and from high-to-low, respectively, in order to check for a delayed equilibrium. The pulse program used was a Hahn echo (interpulse delay 10 µs) with a pre-saturation of the water signal during the repetition delay (d1). As the baseline in the region of interest (methyl groups, 1-2 ppm) is greatly improved with respect to the one-pulse experiment (see figure S2 for comparison), this was the experiment of choice. With our analysis we followed the procedure described by Rice and co-workers.[3]

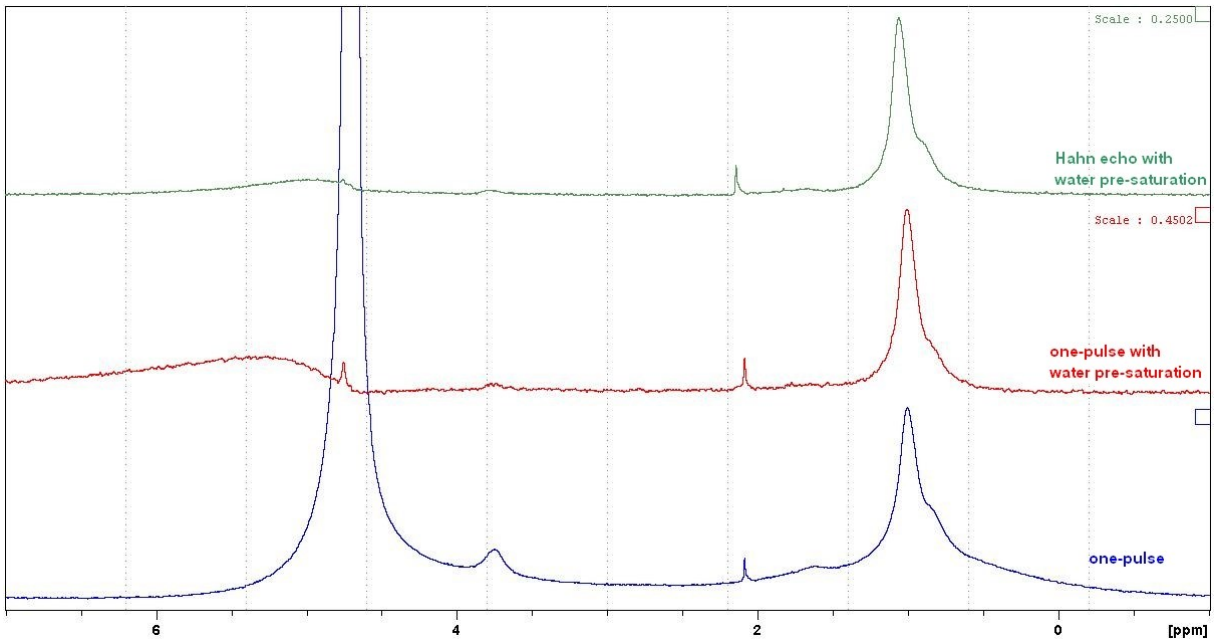

Figure S2: Comparison of ^{1}H NMR spectra of different pulse sequences.

The one-pulse ^{1}H NMR spectrum of the µG was compared with the ^{1}H NMR spectrum of the monomer NIPMAM (Figure S3).

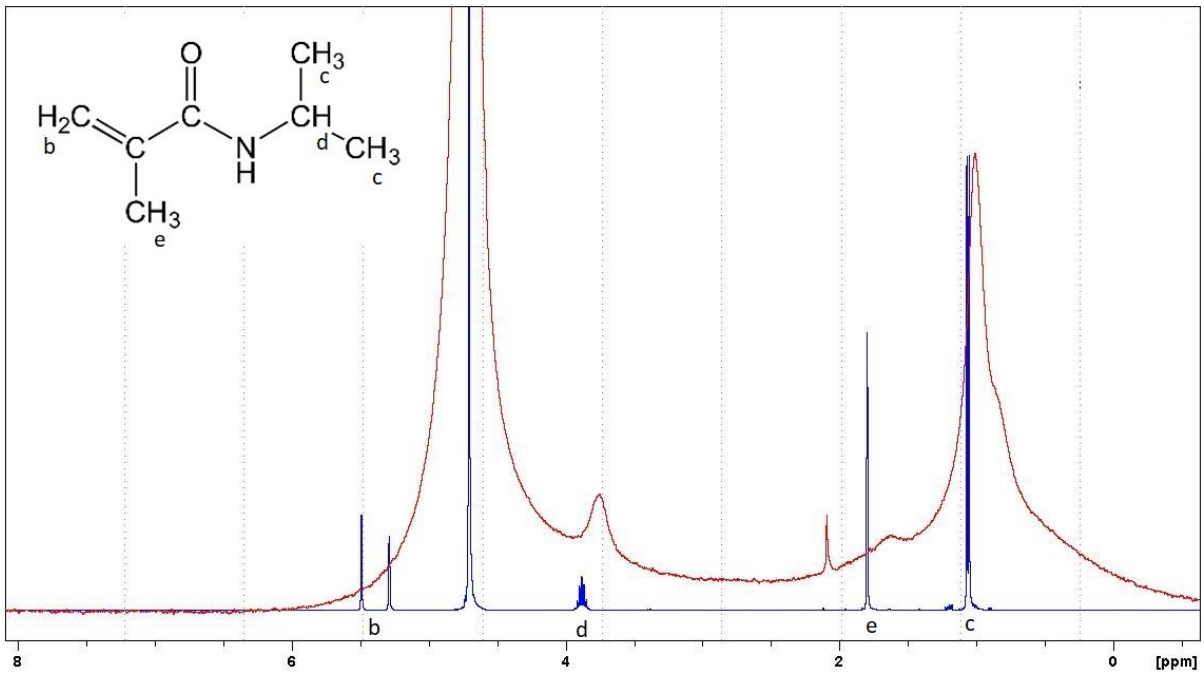

Figure S3: Comparison of ^{1}H NMR spectra of the monomer NIPMAM (blue) and the µG (red).

The peaks in the ^{1}H NMR spectrum of the µG can be assigned to the CH_3-group attached to the chain at 0.8 ppm, to the CH_3-group in the isopropyl group at 1.0 ppm, to the CH_2-group in the chain at 1.6 ppm, and to the CH-group in isopropyl group at 3.8 ppm.[4] We assume that the peak at 2.1 ppm might stem from impurities, e.g. unreacted monomer.

Figure S4 shows the signal evolution with increasing temperature for the µG without salt (the spectra of the other two samples have similar shape). As the experiment is done under deuterium lock on the D_2O signal and the water signal is moving to lower ppm values with temperature, the magnetic field is corrected permanently and the peaks of interest start moving to higher ppm values.

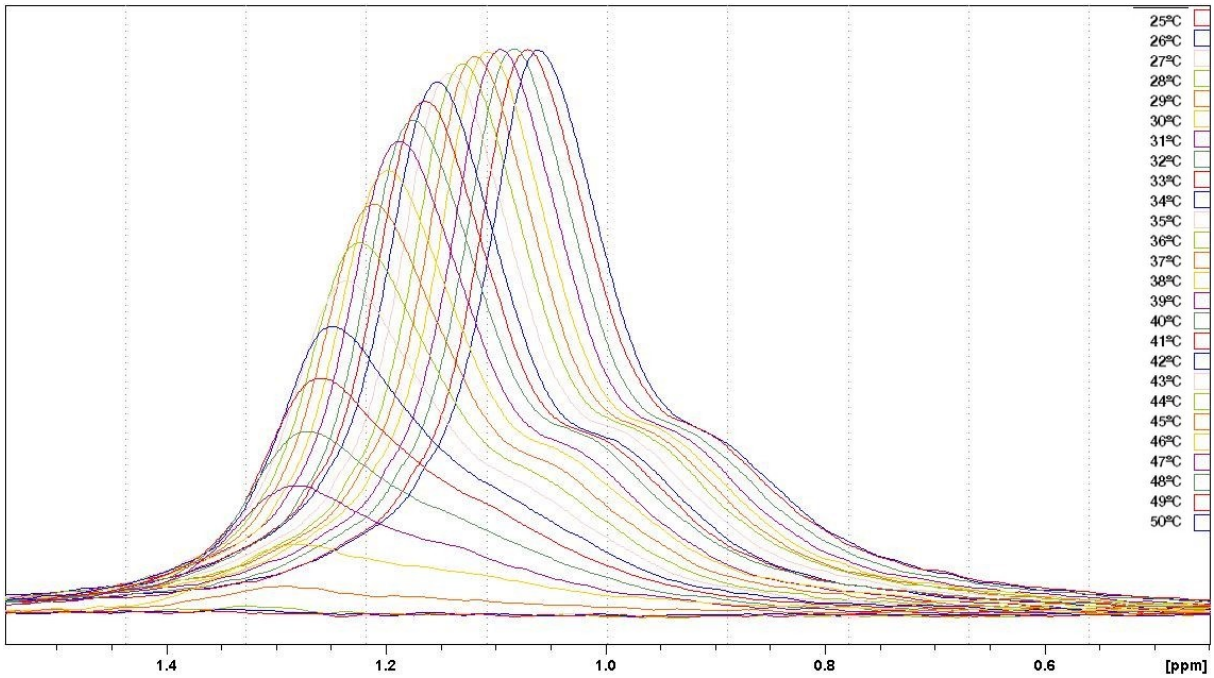

Figure S4: Methyl signal with increasing temperature for the µG dispersion without salt.

The decrease in the intensity of the peaks in Figure S4 can be explained by the collapse of the µG. During the collapse the groups are increasingly restricted in their movement.

Figure S4 depicts the course of the signal intensity as a function of temperature. It can be seen that the peak intensities decrease with increasing temperature. The respective analysis for all three samples is shown in figure S5.

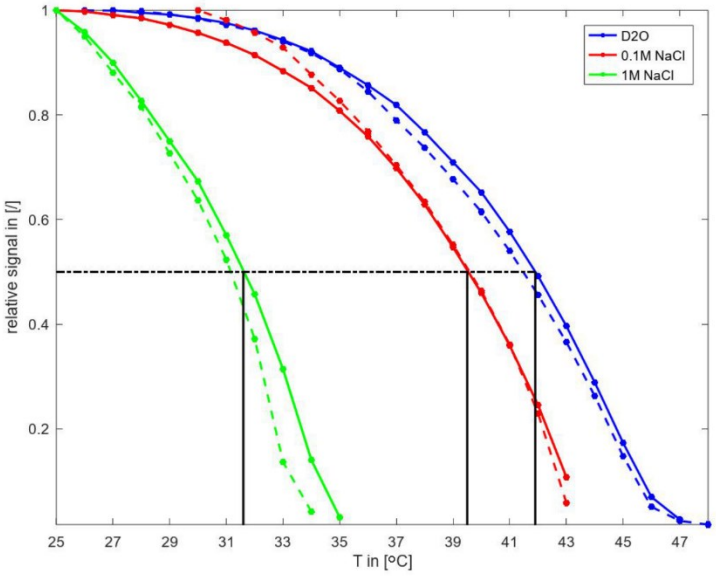

Figure S5: Change in signal intensity as a function of temperature (rising temperature (solid line), declining temperature (dotted line)) for all three samples and indication of the VPTT at half of the signal height.

The temperatures at which the µGs collapse differ significantly in dependency of the NaCl concentration. Without NaCl a relative signal of 0.5 can be detected around 42 °C, with a concentration of 0.1 M it decreases to about 39 °C, and with 1 M NaCl it decreases to about 32 °C.

This could be explained by the 'salting out' effect. The salt leads to a lower energy barrier for the formation of hydrophobic bonds because of a less preferred hydration of hydrophobic molecules.[5,6]

Dye labeling of µGs

The µGs (5 mg) were dispersed in H_2O (0.5 mL, pH 8.5) and dithiothreitol (DTT, Sigma-Aldrich, ≥ 99 %) was added (in H_2O, 0.1 M, pH 8.5). The µGs were purified after 30 min by centrifugation (3 ×, 5.5 krpm, 10 min). They were redispersed in H_2O (1 mL, pH 7.5) and Alexa647-maleimide dye (50 µL, 0.1 mM, Thermo Fisher Scientific) was added. The next day, the dye labeled µGs were purified by centrifugation and redispersed in H_2O.

2. Interactions of non-functionalized µGs with ssDNA

To the µGs (100 µL) Alexa647-labeled $ssDNA_a$ (5'-CGC ATT CAG GAT A_{10}-3'-Alexa647, 10 µL, 0.1 mM, IBA Lifesciences) was added. The salt concentration was adjusted (0 M or 1 M NaCl, respectively). The next day, the µGs were purified by centrifugation (3 ×, 7 krpm, 5-10 min). The µGs were dispersed in H_2O with the corresponding NaCl concentration and heated to 70 °C and purified again.

Fluorescence microscopy with the µGs was performed at room temperature before and after heating them up.

3. DNA-functionalization of µGs

The chosen DNA base sequences were already used by Buchkremer et al. for the build-up of DNA-gold nanoparticle networks.[7] The melting temperatures of the dsDNA was calculated with OligoCalc.[8]

The DNA functionalization was performed with a similar procedure also used for the dye labeling using maleimide terminated $ssDNA_b$ (5'-ATC CTG AAT GCG A_{10}-3'-$(CH_2)_6$-maleimide, 50 µL, 0.1 mM, Biomers) which can hybridize with $ssDNA_a$ due to 12 complementary base pairs. After the purification, the µGs were dispersed in H_2O (1 mL, pH ~ 7.4). The DNA-functionalized µGs were characterized via DLS and zeta-potential measurement.

We further performed electron energy loss spectroscopy (EELS) to analyze the presence of phosphorus after DNA functionalization. The EEL spectra of the DNA functionalized and the pure µGs were measured on a Zeiss Libra 200 FE TEM with an integrated Omega-filter and an alpha tilt of 0° in STEM-Mode. The camera length was 1.2 m and the condensor aperture 20 µm with a spectrum acquisition time of 16 µs per pixel. The core-loss edges of the EEL spectra were extracted by modeling and subtracting the corresponding background region with the Digital Microsoft Software's implemented power-law-command. The corrected spectra are shown in Figure S6.

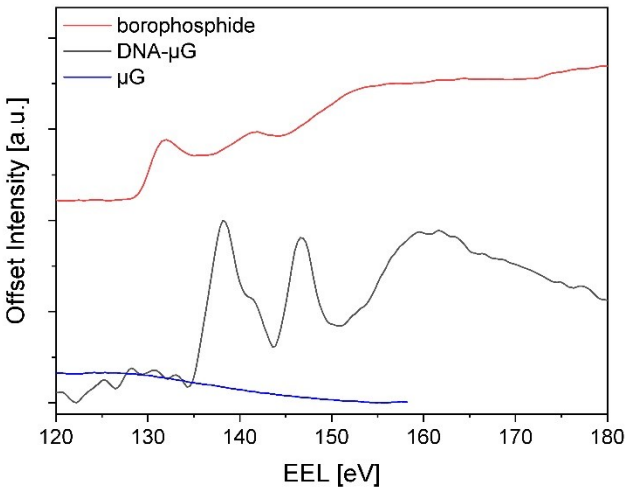

Figure S6: EELS-Spectra of the DNA functionalized and the pure µGs with a spectrum of borophosphide as a reference.

The phosphorus-L-edge is expected around 132 eV [9] and can be found at 134 eV in the spectrum of the DNA functionalized µG. For the pure µG no phosphorus edge can be observed, which was expected as there is no phosphorus in the µG but in the DNA only. In comparison to the reference spectrum the phosphor edge in the spectrum of the functionalized µG is shifted towards higher eV because of the oxidation state of the phosphorus.[10,11] The background noise at lower eV can be explained by the correction of the spectra.

The ssDNA$_b$-functionalized µGs (100 µL) were mixed with complementary, with Alexa647 labeled ssDNA$_a$ (5'-CGC ATT CAG GAT A$_{10}$-3'-Alexa647, 10 µL, 0.1 mM, IBA Lifesciences). The salt concentration was adjusted (0 M, 0.1 M, or 1 M NaCl, repsectively). After the hybridization process overnight, the µGs were purified by centrifugation (3 ×, 7 krpm, 5-10 min). The µGs were dispersed in H_2O with the corresponding NaCl concentration. For the dehybridization process, the µGs were heated up to 50 °C or 70 °C and purified via centrifugation. Fluorescence microscopy was performed at room temperature with the labeled µGs before and after heating them up.

4. Gold nanoparticle µG hybrid systems

Citrate-stabilized AuNPs (diameter d = 12 nm) were synthesized according to the synthesis route of Turkevich et al.[12] The DNA functionalization was performed following the synthesis routes described by Mirkin et al.[13] The citrate-stabilized AuNPs (600 µL, 8 nM) were incubated with thiol-terminated ssDNA$_b$ (5'-CGC ATT CAG GAT A$_{10}$-3'-SH, 50 µL, 0.1 mM, IBA Lifesciences) at 50 °C for 24 h. Within three days, they were brought stepwise to a final concentration of 0.01 M phosphate and 0.1 M NaCl. The DNA-functionalized AuNPs were purified by centrifugation (3 ×, 13.5 krpm, 20 min, 10 °C) and re-dispersed in PBS (10 mM phosphate, 0.1 M NaCl, pH 7.4).

The DNA-functionalized AuNP (100 µL, ca. 3 nM) were added to the DNA-functionalized µGs (25 µL, 5 mg/mL) and stored overnight at 4 °C. These hybrids were separated from the single particles by centrifugation (5 krpm, 20 min, 10 °C).

For the release of the AuNPs from the Hybrids, the hybrid system was heated up over the melting temperature of the dsDNA.

The hybrid systems were characterized by electron microscopy with a FE-SEM LEO/Zeiss Supra 35 VP on copper grids (Plano) in SEM and SEM-T mode.

5. UV-Vis spectroscopy

The hybrid systems were characterized by means of UV-Vis spectroscopy. The spectra were measured between 300 and 800 nm against water in 1 nm steps at a Jasco V-630 spectrophotometer. The measurements were performed below and above T_{VPT}, but always below T_m. For a comparison, the DNA$_b$-functionalized µGs were measured under the same conditions. The raw spectra are shown in Figure S2.

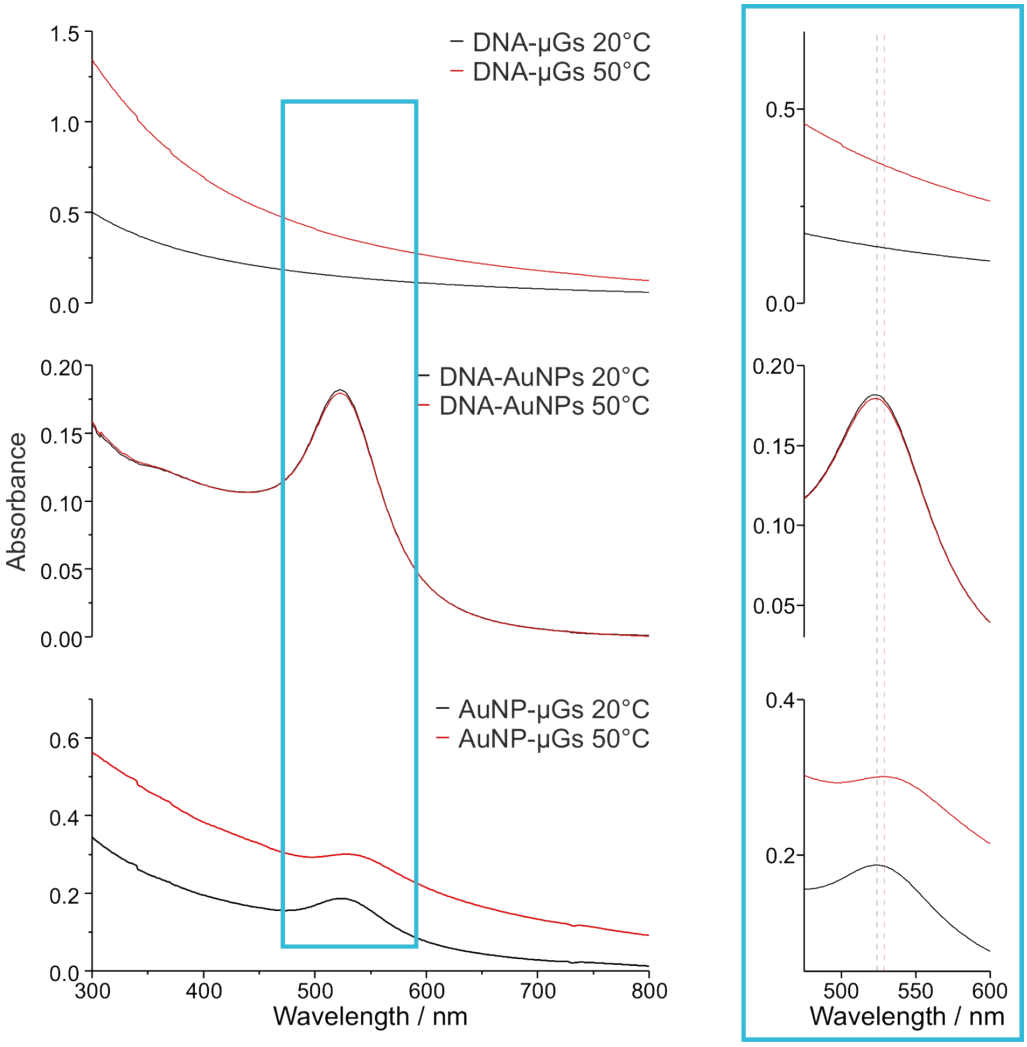

Figure S2: UV-Vis spectra at $T < T_{VPT}$ (20 °C) and $T_{VPT} < T$ (50 °C) of the DNA-µGs (top), the DNA-functionalized AuNPs with a plasmon band at 523 nm, which is not affected by the temperature change (middle) and the UV-Vis spectra of the AuNP-loaded-µGs (bottom). At 20 °C the maximum is at 524 nm and at 50 °C, above the T_{VPT}, it broadens, and the maximum is shifted to 529 nm.

The high scattering of the µGs above T_{VPT} required a background correction to correctly access the plasmon bands and their maxima as shown in Figure 3 of the mansucript. For the DNA-functionalized AuNPs the maximum shifts only very slightly from 525 nm to 526 nm. In contrast, for the hybrid system a shift from 529 nm to 542 nm became obvious in the corrected spectra due to an enhanced plasmon coupling in the collapsed state of the µG.

6. Tomography of AuNP-µG hybrids

A FEI Tecnai F20 transmission electron microscope at an acceleration voltage of 200 kV was used for the electron tomography. The sample was fixed to a Gatan 916 high tilt tomography holder and investigated in TEM imaging mode in order to gain contrasts from both the Au nanoparticles and the microgel. Tilt series with 147 projections in a maximum tilt-angle range of ±73° were acquired. Reconstruction of the 3D structure was performed with Tomoviz[14] using the weighted back projection (WBP) algorithm. A Python package Trackpy[15] was used for locating the AuNPs.

7. Fluorescence microscopy

The investigated microgels where visualized on a commercial inverted microscope (Nikon Eclipse Ti-E). Fluorescence was collected with a 100×/1.40 NA oil immersion objective (HP PLAN, Nikon) and imaged on a CMOS camera (Photometrics, PRIME 95B). As the microgels have a hydrodynamic radius of approx. 400 nm, they are large enough to be observed in the transmission (bright-field) mode. To measure the fluorescence microscopy image, we used a 640 nm laser (Toptica iBeam smart 640CD) with a laser power of 200 mW, which we use at max. 9% of the laser power. In most cases we overlaid the transmission image and the fluorescence microscopy image at the same field of view in order to gain correlated information.

8. Super-resolution fluorescence microscopy

The investigated µGs were visualized using 3D SRFM techniques. We used a commercial inverted microscope (Nikon Eclipse Ti-E). Fluorescence was collected with a 100×/1.40 NA oil immersion objective (HP PLAN, Nikon) and imaged on a CMOS camera (Photometrics, PRIME 95B). As already reported in our previous publications,[1] we employed the well-established dSTORM technique.[16] For 3D localizations, we implemented the double-helix point spread function (DH-PSF) method using a double Helix SPINDLE™ module (Double Helix LLC, Boulder). 3D information was acquired from the z-dependent rotation angle of the two lobes by which a single object is imaged after the emission light passes an appropriate phase mask.[1, 17] All experiments were conducted in quasi total internal reflection mode (qTIRF) restricting the excitation volumes to a few hundred nanometers from the slide surface. The µGs were labeled with Alexa647 and the appropriate blinking conditions were achieved with a 50 mM cysteamine blinking buffer.

9. References

[1] L. Hoppe Alvarez, S. Eisold, R. A. Gumerov, M. Strauch, A. A. Rudov, P. Lenssen, D. Merhof, I. I. Potemkin, U. Simon, D. Wöll, Nano Lett. **2019**, 19, 8862-8867.

[2] J. C. Gaulding, M. H. Smith, J. S. Hyatt, A. Fernandez-Nieves, L. A. Lyon, Macromolecules **2012**, 45, 39-45.

[3] C. M. Burba, S. M. Carter, K. J. Meyer, C. V. Rice, J. Phys. Chem. B **2008**, 112, 10399–10404.

[4] C. Rice Biomacromolecules 2006, 7, 2923-2925.

[5] C. M. Burba, S. M. Carter, K. J. Meyer, C. V. Rice, J. Phys. Chem. B **2008**, 112, 10399–10404,

[6] Y. Zhang, S. Furyk, D. E. Bergbreiter, P. S. Cremer J. Am. Chem. Soc. **2005**, 127 (41), 14505-14510

[7] A. Buchkremer, M. J. Linn, J. U. Timper, T. Eckert, J. Mayer, W. Richtering, G. von Plessen, U. Simon, J. Phys. Chem. C **2014**, 118, 7174-7184.

[8] W. A. Kibbe, Nucleic Acids Res. **2007**, 35, W43-W46.

[9] https://eels.info/atlas/phosphorus

[10] R. F. Egerton, Electron Energy-Loss Spectroscopy in the Electron Microscope, **2011**, Springer US p.204.

[11] M. Rei Vilar, A. M. Botelho do Rego, A. M. Ferraria, Y. Jugnet, C. Nogués, D. Peled, R. Naaman J. Phys. Chem. B **2008**, 112 (23), 6957-6964]

[12] J. Turkevich, P. C. Stevenson, J. Hillier, J. Phys. Chem. **1953**, 57, 670-673.

[13] a) C. A. Mirkin, R. L. Letsinger, R. C. Mucic, J. J. Storhoff, Nature **1996**, 382, 607-609; b) J. J. Storhoff, R. Elghanian, R. C. Mucic, C. A. Mirkin, R. L. Letsinger, J. Am. Chem. Soc. **1998**, 120, 1959-1964.

[14] https://tomviz.org

[15] D. Allan, C. van der Wel, N. Keim, T. A. Caswell, D. Wieker, R. Verweij, C. Reid, Thierry, L. Grueter, K. Ramos, apiszcz, zoeith, R. W. Perry, F. Boulogne, P. Sinha, pfigliozzi, N. Bruot, L. Uieda, J. Katins, H. Mary, A. Ahmadia, soft-matter/trackpy: Trackpy v0.4.2 ed., Zenodo, https://doi.org/10.5281/zenodo.1213240, **2019**.

[16] a) M. Heilemann, S. van de Linde, M. Schüttpelz, R. Kasper, B. Seefeldt, A. Mukherjee, P. Tinnefeld, M. Sauer, Angew. Chem. Int. Ed. **2008**, 47, 6172-6176; b) D. R. Whelan, T. Holm, M. Sauer, T. D. M. Bell, Aust. J. Chem. **2014**, 67, 179-183.

[17] a) S. R. P. Pavani, R. Piestun, Opt. Express **2008**, 16, 22048-22057; b) S. R. P. Pavani, M. A. Thompson, J. S. Biteen, S. J. Lord, N. Liu, R. J. Twieg, R. Piestun, W. E. Moerner, Proc. Natl. Acad. Sci. U.S.A. **2009**, 106, 2995-2999.